Available online at www.sciencedirect.com

ScienceDirect

IFAC PapersOnline CONFERENCE PAPER ARCHIVE

IFAC PapersOnLine 53-1 (2020) 500–505

Nonlinear Model Predictive Control for an Exothermic Reaction in an Adiabatic CSTR

Morten Ryberg Wahlgreen * **Eskild Schroll-Fleischer** * **Dimitri Boiroux** * **Tobias K. S. Ritschel** ** **Hao Wu** *** **Jakob Kjøbsted Huusom** *** **John Bagterp Jørgensen** *

* *Department of Applied Mathematics and Computer Science, Technical University of Denmark, DK-2800 Kgs. Lyngby, Denmark*
** *2-control ApS, DK-2800 Kgs. Lyngby, Denmark*
*** *Department of Chemical and Biochemical Engineering, Technical University of Denmark, DK-2800 Kgs. Lyngby, Denmark*

Abstract: We model and simulate an exothermic reaction conducted in an adiabatic continuous stirred tank reactor (CSTR). The system has multiple steady states in part of its operating window. We demonstrate that the three-state model representing the mass and energy balances of the system can be well approximated with a two-state as well as a one-state model. The reduced-order models are relevant for efficient implementation of nonlinear model predictive control (NMPC). We extend the drift term in the system of deterministic ordinary differential equations (ODEs) with a diffusion term such that the process is modeled by a system of stochastic differential equations (SDEs). The SDE representation is well-suited for development of the NMPC that is based on a continuous-discrete extended Kalman filter (CD-EKF) and an optimal control problem. The optimal control problem (OCP) is solved using a multiple-shooting algorithm as the NMPC must be able to stabilize the system at stable as well as unstable steady states. Simulations demonstrate that the NMPC based on a one-state reduced SDE can track any reactor temperature setpoint at stable as well as unstable steady states.

Keywords: Nonlinear model predictive control, Multiple steady states, Adiabatic continuous stirred tank reactor, Exothermic reaction, Stochastic differential equations

1. INTRODUCTION

For many processes, the process industries use linear model predictive control (LMPC) based on data-driven models (step response models) extensively (Qin and Badgwell, 2003; Forbes et al., 2015; Honc et al., 2016). However, MPC based on linear models are unable to track highly nonlinear dynamical systems such as chemical reactor dynamics with multiple steady states and where the sign of the gain may change. Nonlinear model predictive control (NMPC) must be used to track the setpoints of such systems. The reported industrial applications of nonlinear model predictive control (NMPC) based on first-principle models with parameters estimated from data are scarce and mostly related to polymerization processes (Bindlish, 2015). To demonstrate that chemical reactors with complex dynamics may benefit from NMPC, we use a classical exothermic reaction conducted in an adiabatic continuous stirred tank reactor (CSTR) (Vejtasa and Schmitz, 1970; Schroll-Fleischer et al., 2017).

In this paper, we develop the model of this reactor and demonstrate how model order reduction based on process insight may reduce the model from a three state model to a one state model. We provide nonlinear analysis of the model and demonstrate that the model has multiple steady states in part of its operating window. Furthermore, we compare the deterministic solution obtained solving a system of ordinary differential equations (ODEs) to a realization of the stochastic system represented by stochastic differential equations (SDEs). The reduced-order one-state continuous-time SDE system along with an output equation and a measurement equation observed at discrete-times forms a continuous-discrete time system that is used for design of the NMPC (Boiroux and Jørgensen, 2018; Brok et al., 2018; Ritschel and Jørgensen, 2019). The NMPC consists of a continuous-discrete extended Kalman filter (CD-EKF) and an optimal control problem (OCP) with input constraints. The key novelties in this paper are the reduced order one-state model and the demonstration that an NMPC based on an SDE representation of the one-state model may track any temperature setpoint in the operating window.

While the results in this paper are based on simulations, our goal is not only to provide another simulation study. Rather, we have built a laboratory version of this reaction system (Schroll-Fleischer et al., 2017), and the results in this paper serves as the first step in the practical

⋆ The work in this paper is partially funded by the EC in the COCOP project, EUDP in the IEA Energy Efficient Process Control project, and Innovation Fund Denmark in the CITIES project. Corresponding author: J.B. Jørgensen (E-mail: jbjo@dtu.dk).

10.1016/j.ifacol.2020.06.084

Table 1.

Density	ρ	1.0	kg/L
Specific heat capacity	c_P	4.186	kJ/(kg·K)
Arrhenius constant	k_0	exp(24.6)	L/(mol·s)
Activation energy	E_a/R	8500	K
Reaction enthalpy	ΔH_r	−560	kJ/mol
Reactor volume	V	0.105	L
Inlet concentration of A	$C_{A,in}$	1.6/2	mol/L
Inlet concentration of B	$C_{B,in}$	2.4/2	mol/L
Inlet temperature	T_{in}	273.65	K
		= 0.5	°C

realization of NMPC algorithms for nonlinear chemical processes that can be transfered into industrial practice.

The remaining part of this paper is organized as follows. Section 2 presents the process model, presents reduced order models, and demonstrates the behavior of these models of the process by simulation. The components of the NMPC algorithm are presented in Section 3. First, Section 3 presents the continuous-discrete stochastic model that is used by the NMPC in the CD-EKF and the OCP. Section 3.1 presents the CD-EKF, Section 3.2 presents the regulator in the NMPC, and Section 3.3 demonstrates the performance of NMPC by closed-loop simulations. Section 4 contains the conclusion.

2. PROCESS MODELING AND SIMULATION

This section presents the chemical model (stoichiometry, kinetics and thermodynamics) and the process model (mass and energy balances). Steady state analysis demonstrates that the model has multiple steady states in part of the operating window. We demonstrate that the three state model of the system may be well approximated by a two-state as well as a one-state model. We also develop equivalent SDE models and do a numerical phase plane analysis. Table 1 lists the parameters for the adiabatic CSTR.

2.1 Reaction stoichiometry, kinetics, and thermodynamics

We consider an exothermic reaction,

$$A + 2B \rightarrow \frac{1}{2}C + \frac{1}{2}D + 2E. \tag{1}$$

r denotes the rate of reaction for (1) and ΔH_r denotes the corresponding reaction enthalpy.

The rate of reaction is

$$r = r(C_A, C_B, T) = k(T) C_A C_B, \tag{2}$$

where the rate constant, $k(T)$, is defined by the Arrhenius expression

$$k(T) = k_0 \exp\left(\frac{-E_a}{RT}\right). \tag{3}$$

We define the production rate of A and B from the stoichiometry (1):

$$R_A = R_A(C_A, C_B, T) = -r(C_A, C_B, T), \tag{4a}$$
$$R_B = R_B(C_A, C_B, T) = -2r(C_A, C_B, T). \tag{4b}$$

Using a similar concept, we define the rate of temperature change due reaction enthalpy (production rate of temperature) as

$$R_T = R_T(C_A, C_B, T) = \beta r(C_A, C_B, T), \tag{5}$$

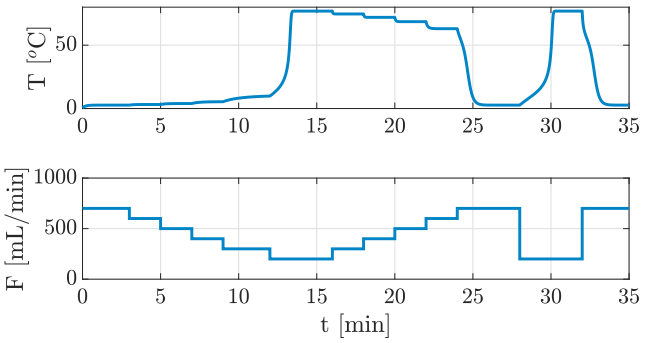

Fig. 1. The simulated reactor temperature, T, for a specified flow rate trajectory, F.

where $\beta = -\Delta H_r/(\rho c_P)$ is defined from the enthalpy of reaction, ΔH_r. ρ denotes the density of the aqueous mixture and c_P denotes the specific heat capacity.

2.2 Mass and energy balances

Mass and energy balance considerations of the constant volume reactor yield the following system of ODEs

$$\dot{C}_A = \frac{F}{V}(C_{A,in} - C_A) + R_A(C_A, C_B, T), \tag{6a}$$
$$\dot{C}_B = \frac{F}{V}(C_{B,in} - C_B) + R_B(C_A, C_B, T), \tag{6b}$$
$$\dot{T} = \frac{F}{V}(T_{in} - T) + R_T(C_A, C_B, T). \tag{6c}$$

B is the limiting reactant and the extent of reaction, X, can therefore be defined as

$$X = \frac{C_{B,in} - C_B}{C_{B,in}} = 1 - \frac{C_B}{C_{B,in}}. \tag{7}$$

From (7) it is clear that $X \in [0, 1]$.

2.3 Steady state analysis

The steady state of (6) is the solution to the nonlinear system of equations

$$\frac{F_s}{V}(C_{A,in} - C_{As}) - r(C_{As}, C_{Bs}, T_s) = 0, \tag{8a}$$
$$\frac{F_s}{V}(C_{B,in} - C_{Bs}) - 2r(C_{As}, C_{Bs}, T_s) = 0, \tag{8b}$$
$$\frac{F_s}{V}(T_{in} - T_s) + \beta r(C_{As}, C_{Bs}, T_s) = 0. \tag{8c}$$

From (8), the rate of reaction, r, can be isolated,

$$\begin{aligned} r(C_{As}, C_{Bs}, T_s) &= \frac{F_s}{V}(C_{A,in} - C_{As}) \\ &= \frac{1}{2}\frac{F_s}{V}(C_{B,in} - C_{Bs}) \\ &= -\frac{1}{\beta}\frac{F_s}{V}(T_{in} - T_s), \end{aligned} \tag{9}$$

such that the steady concentrations, C_{As} and C_{Bs}, can be expressed as function of the steady state temperature, T_s,

$$C_{As} = C_{As}(T_s) = C_{A,in} + \frac{1}{\beta}(T_{in} - T_s), \tag{10a}$$
$$C_{Bs} = C_{Bs}(T_s) = C_{B,in} + \frac{2}{\beta}(T_{in} - T_s). \tag{10b}$$

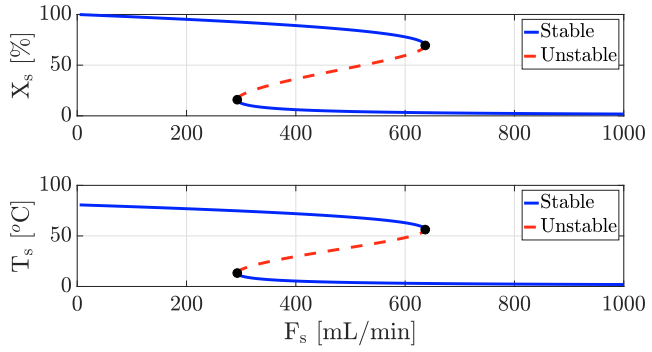

Fig. 2. Steady state extent of reaction, X_s, and temperature, T_s, as function of the flow rate, F_s.

Similarly, the steady state extent of reaction, X_s, can be expressed as a function of the steady state temperature, T_s,

$$X_s = X_s(T_s) = \frac{C_{B,in} - C_{Bs}}{C_{B,in}} = \frac{-2}{\beta C_{B,in}}(T_{in} - T_s). \quad (11)$$

The steady state temperature, T_s, may be determined by solution of the nonlinear system of equations (8), or by solution of the scalar equation

$$\frac{F_s}{V}(T_{in} - T_s) + R_T(C_{As}(T_s), C_{Bs}(T_s), T_s) = 0. \quad (12)$$

Notice that using (11) and (12) we get

$$T_s = T_{in} + \frac{1}{2}\beta C_{B,in} X_s, \quad (13a)$$

$$F_s = V\frac{R_T(C_{As}(T_s), C_{Bs}(T_s), T_s)}{T_s - T_{in}}, \quad (13b)$$

such that the steady state flow rate, F_s, can be determined from the steady state temperature, T_s, chosen such that $0 \leq C_{As}(T_s) \leq C_{A,in}$ and $0 \leq C_{Bs}(T_s) \leq C_{B,in}$. Since B is the limiting reactant, this is the same as choosing the steady state extent of reaction, X_s, as $0 \leq X_s \leq 1$. This implies that $T_s \in]T_{in}, T_{\max}]$, where the lower limit, T_{in}, is attained for an infinite flow rate, F_s, and the upper limit is obtained when the limiting reactant is fully converted, i.e. $X_s = 1$ and $C_{Bs} = 0$ mol/L, such that $F_s = 0$ mL/min. Consequently, $X_s \in]0, 1]$, $T_s \in]T_{in}, T_{\max}]$, where

$$T_{\max} = T_{in} + \frac{1}{2}\beta C_{B,in}, \quad (14)$$

and $F_s \in [0, \infty[$. In practice, an infinite flow rate is not achievable. Therefore, $F_s \in [0, F_{\max}]$ such that $X_s > 0$ and $T_s > T_{\min}$. In this way, the steady state curve (see Fig. 2) can be computed efficiently by gridding the extent of reaction, X_s between 0 and 1, computing the corresponding steady state temperature, T_s, steady state concentrations, C_{As} and C_{Bs}, and steady state flow rate, F_s. As is evident in Fig. 2, this process has multiple steady states in the operation window $F_s \in [0, 1000]$ mL/min.

Using (11), the steady state temperature, T_s, can be related to the steady state extent of reaction, X_s, by (13a) such that the steady state concentrations, C_{As} and C_{Bs}, in (10) is expressed as a function of the steady state extent of reaction, X_s:

$$C_{As} = C_{As}(X_s) = C_{B,in}\left(\frac{C_{A,in}}{C_{B,in}} - \frac{1}{2}X_s\right), \quad (15a)$$

$$C_{Bs} = C_{Bs}(X_s) = C_{B,in}(1 - X_s). \quad (15b)$$

Define the extent of reaction production rate as

$$R_X = R_X(C_A, C_B, T) = -\frac{1}{C_{B,in}} R_B(C_A, C_B, T) \quad (16)$$

Rewrite (8b) and (8c) by application of (15) and (16):

$$-\frac{F_s}{V}X_s + R_X(C_{As}(X_s), C_{Bs}(X_s), T_s) = 0, \quad (17a)$$

$$\frac{F_s}{V}(T_{in} - T_s) + R_T(C_{As}(X_s), C_{Bs}(X_s), T_s) = 0. \quad (17b)$$

This is a two-dimensional system of equations. Given F_s, it can be used to compute the pair (X_s, T_s). In turn, C_{As} and C_{Bs} can be determined by (15). The solution, (C_{As}, C_{Bs}, T_s), obtained from the three dimensional model, (8), is identical to the solution obtained from the two dimensional model, (17) and (15), as well as the one dimensional model, (12) and (10).

2.4 Model order reduction

While the one- and two-state reduced order models are exact equivalents to the full three-dimensional model at steady state, the same model structures can also be used to approximate the dynamic behavior of the system as the trajectories approach a one-dimensional manifold.

Notice that the extent of reaction (7) and the mass balance for component B (6b) imply

$$\dot{C}_B = \frac{F}{V}C_{B,in}X + R_B(C_A, C_B, T), \quad (18a)$$

$$\dot{X} = -\frac{1}{C_{B,in}}\dot{C}_B, \quad (18b)$$

such that the assumption that the concentration of C_A is related to the extent of reaction

$$C_A = C_A(X) = C_{B,in}\left(\frac{C_{A,in}}{C_{B,in}} - \frac{1}{2}X\right), \quad (19a)$$

$$C_B = C_B(X) = C_{B,in}(1 - X), \quad (19b)$$

gives the two-dimensional model

$$\dot{X} = -\frac{F}{V}X + R_X(C_A(X), C_B(X), T), \quad (20a)$$

$$\dot{T} = \frac{F}{V}(T_{in} - T) + R_T(C_A(X), C_B(X), T), \quad (20b)$$

where R_X is determined by (16) and R_T is determined by (5). This two-dimensional model is equivalent to the three-dimensional model of the system provided C_A has approached the manifold determined by (19a). The relation (19b) is an exact relation provided by the definition of the extent of reaction (7).

Further, inspired by (9) and (10), the concentrations of A and B, C_A and C_B, may be approximated by

$$C_A = C_A(T) = C_{A,in} + \frac{1}{\beta}(T_{in} - T), \quad (21a)$$

$$C_B = C_B(T) = C_{B,in} + \frac{2}{\beta}(T_{in} - T), \quad (21b)$$

such that the evolution of the system can be described by the one-state differential equation

$$\dot{T} = \frac{F}{V}(T_{in} - T) + R_T(C_A(T), C_B(T), T), \quad (22)$$

where R_T is determined by (5). In this case the extent of reaction, X, is computed by

$$X = X(T) = \frac{C_{B,in} - C_B(T)}{C_{B,in}} = \frac{-2}{\beta C_{B,in}}(T_{in} - T). \quad (23)$$

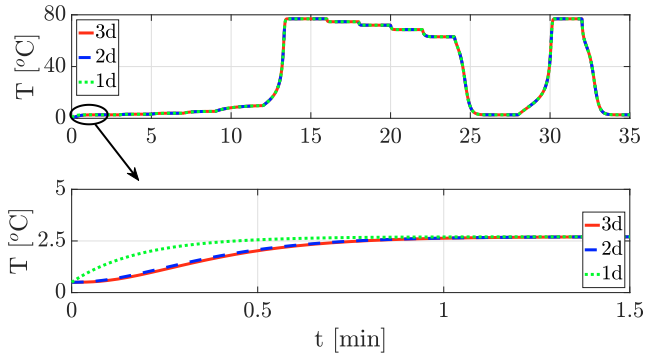

Fig. 3. Comparison of models for the scenario in Fig. 1.

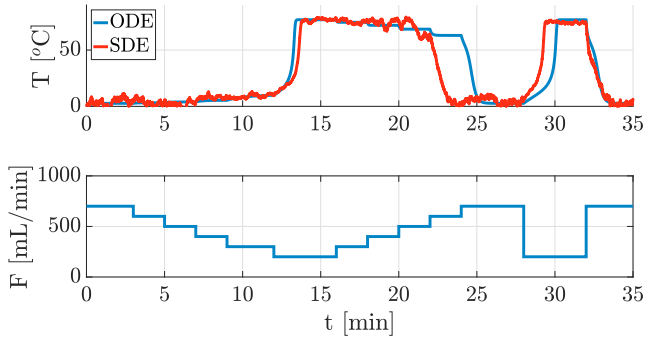

Fig. 4. Open loop simulation of a three-state model as an ODE system and as an SDE system for the scenario in Fig. 1.

Fig. 3 illustrates the temperature evolution simulated by the three-, the two-, and the one-dimensional model. All three models converge to the same one-dimensional manifold after approximately 1 min. For the initial conditions in the simulated scenario (3d: $[C_A, C_B, T]_0 = (0, 0, T_{in})$, 2d: $[X, T]_0 = [1, T_{in}]$, 1d: $T_0 = T_{in}$), the two-state model is a very good approximation everywhere to the three-state model. The simulations in Fig. 3 indicate that all models converge to the one-dimensional manifold (1d model), but the initial conditions of the three- and two-dimensional model are not necessarily on this manifold. To be on this manifold, the initial conditions must be $C_{A0} = C_A(T_0)$, $C_{B0} = C_B(T_0)$ and $X_0 = X(T_0)$ as determined by (21) and (23).

The implication of this model-order reduction is that the NMPC may use a one-dimensional model rather than a three-dimensional model for its filtering and prediction. Also the two-dimensional model provides an accurate approximation for phase plane analysis of the system.

2.5 Stochastic differential equation system

The deterministic model (6) may be extended by a stochastic term describing the random variations in the inputs to the process. This results in a system of SDEs. The SDE representation is important for sensitivity analysis and assessment of the effect of uncertainties on the system. The stochastic representation is also important for design of the state estimator in the NMPC.

Assuming that the stochastic variations are related to the inlet temperature, the SDE equivalent of the three state model is

$$\mathrm{d}C_A = \left(\frac{F}{V}(C_{A,in} - C_A) + R_A(C_A, C_B, T)\right)\mathrm{d}t, \quad (24a)$$

$$\mathrm{d}C_B = \left(\frac{F}{V}(C_{B,in} - C_B) + R_B(C_A, C_B, T)\right)\mathrm{d}t, \quad (24b)$$

$$\mathrm{d}T = \left(\frac{F}{V}(T_{in} - T) + R_T(C_A, C_B, T)\right)\mathrm{d}t + \frac{F}{V}\sigma_T \mathrm{d}\omega(t), \quad (24c)$$

where $\mathrm{d}\omega(t) \sim N_{iid}(0, I\mathrm{d}t)$. Similarly, the SDE equivalent of the one-state model becomes

$$\mathrm{d}T = \left(\frac{F}{V}(T_{in} - T) + R_T(C_A(T), C_B(T), T)\right)\mathrm{d}t + \frac{F}{V}\sigma_T \mathrm{d}\omega(t). \quad (25)$$

The model (24) is used for simulation of the system, while (25) is used in the design of the NMPC. Fig. 4 illustrates one realization of the temperature solution to (24) and compares it to the solution of (6).

2.6 Phase portrait

Fig. 5 shows the phase portrait for the two-state model (20) at different flow rates. Notice the separatrix for the flow rate with multiple steady states.

3. NMPC ALGORITHM AND SIMULATION

The NMPC is based on the continuous-discrete stochastic system,

$$\mathrm{d}x(t) = f(x(t), u(t), p)\mathrm{d}t + \sigma(x(t), u(t), p)\mathrm{d}\omega(t), \quad (26a)$$

$$y(t_k) = \bar{y}(t_k) + v(t_k) = g(x(t_k), p) + v(t_k), \quad (26b)$$

$$z(t) = h(x(t), p), \quad (26c)$$

where $\mathrm{d}\omega(t) \sim N_{iid}(0, I\mathrm{d}t)$ and $v(t_k; p_v) \sim N_{iid}(0, R_k)$ with $R_k = R_v(t_k, p)$. x denotes the states, y denotes the measurements, z denotes the outputs, u denotes the manipulated inputs, and p denotes the parameter vector. We use the one-state SDE model (25) to represent the dynamics (26a). The measurement, y, is the temperature, T, corrupted by measurement noise. The temperature, T, is also the output, z. The measurement noise covariance is $R_v(t_k, p) = \sigma_v^2$ and the parameter vector is $p = [\beta; k_0; E_a/R; V; C_{A,in}; C_{B,in}; T_{in}; \sigma_T; \sigma_v]$ with the parameters in Table 1, $\sigma_T = 5$, and $\sigma_v = 0.15$. The parameter vector can be estimated from data.

3.1 Continuous-discrete extended Kalman filter

The NMPC uses a CD-EKF based on (26) to compute the filtered state estimate, $\hat{x}_{k|k}$, and its covariance, $P_{k|k}$. The CD-EKF computes the filtered state-covariance pair, $(\hat{x}_{k|k}, P_{k|k})$, based on the previous filtered state-covariance pair, $(\hat{x}_{k-1|k-1}, P_{k-1|k-1})$, the current measurement, y_k, and previous manipulated variable, u_{k-1}, by doing a one-step prediction and filtering.

One-step prediction The one-step prediction,

$$\hat{x}_{k|k-1} = \hat{x}_{k-1}(t_k), \quad (27a)$$

$$P_{k|k-1} = P_{k-1}(t_k), \quad (27b)$$

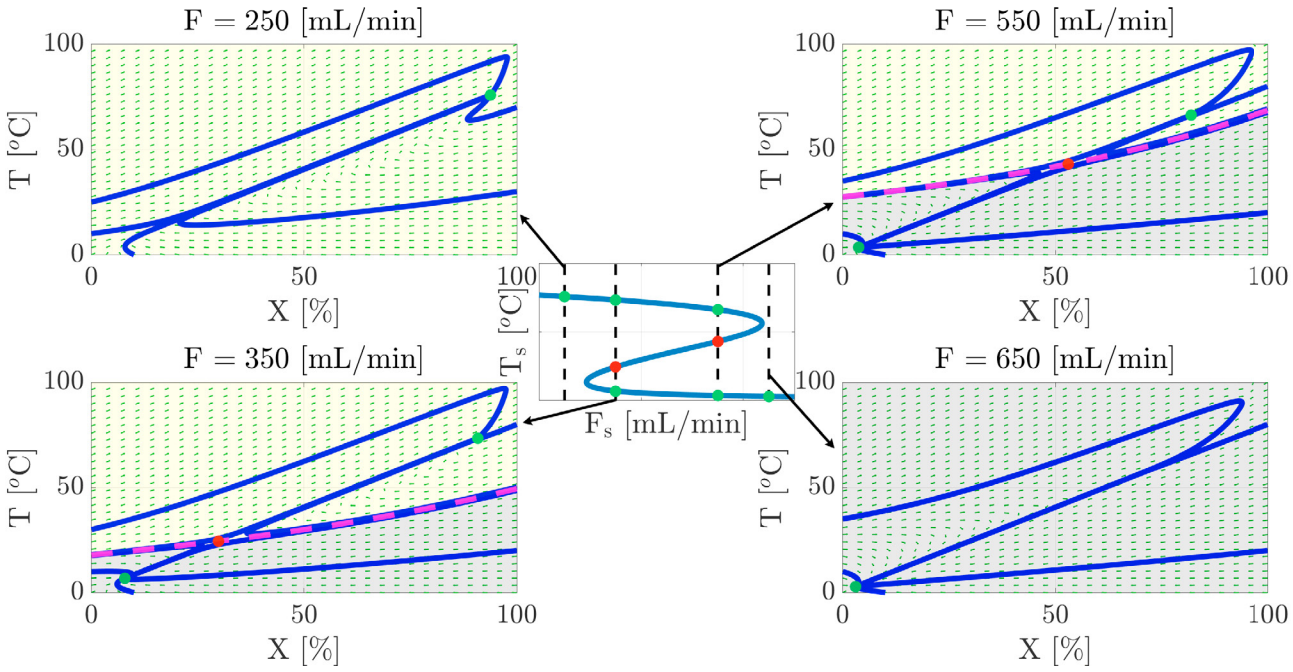

Fig. 5. Steady states for four different flow rates and the associated phase portrait for each flow rate. The phase portraits has an indicator for the stability of the steady states (green for stable and red for unstable). The blue curves show a couple of trajectories and the separatrix is indicated in magenta. The separatrix indicates which steady state a given initial state will lead to. Labels: T = Temperature, X = Extent of Reaction, F = Flow.

is obtained as the solution to

$$\frac{\mathrm{d}}{\mathrm{d}t}\hat{x}_{k-1}(t) = f(\hat{x}_{k-1}(t), u_{k-1}, p), \tag{28a}$$

$$\frac{\mathrm{d}}{\mathrm{d}t}P_{k-1}(t) = A_{k-1}(t)P_{k-1}(t) + P_{k-1}(t)A_{k-1}(t)' + \sigma_{k-1}(t)\sigma_{k-1}(t)', \tag{28b}$$

solved for $t \in [t_{k-1}, t_k]$ with the initial condition

$$\hat{x}_{k-1}(t_{k-1}) = \hat{x}_{k-1|k-1}, \tag{29a}$$

$$P_{k-1}(t_{k-1}) = P_{k-1|k-1}, \tag{29b}$$

and

$$A_{k-1}(t) = \frac{\partial f}{\partial x}(\hat{x}_{k-1}(t), u_{k-1}, p), \tag{30a}$$

$$\sigma_{k-1}(t) = \sigma(\hat{x}_{k-1}(t), u_{k-1}, p). \tag{30b}$$

Filtering The CD-EKF computes the filtered states, $\hat{x}_{k|k}$, from the one-step prediction, $\hat{x}_{k|k-1}$, its covariance, $P_{k|k-1}$, and the measurement, y_k,

$$\hat{y}_{k|k-1} = g(\hat{x}_{k|k-1}, p), \quad C_k = \frac{\partial}{\partial x}g(\hat{x}_{k|k-1}, p), \tag{31a}$$

$$e_k = y_k - \hat{y}_{k|k-1}, \quad R_{e,k} = R_k + C_k P_{k|k-1} C_k', \tag{31b}$$

$$\hat{x}_{k|k} = \hat{x}_{k|k-1} + K_k e_k, \quad K_k = P_{k|k-1}C_k' R_{e,k}^{-1}. \tag{31c}$$

The covariance, $P_{k|k}$, is computed by

$$P_{k|k} = P_{k|k-1} - K_k R_{e,k} K_k' \tag{32a}$$

$$= (I - K_k C_k)P_{k|k-1} \tag{32b}$$

$$= (I - K_k C_k)P_{k|k-1}(I - K_k C_k)' + K_k R_k K_k'. \tag{32c}$$

Even though (32a) is computationally cheaper, (32c) is the preferred form as it guarantees the filtered covariance to be symmetric and positive semi-definite (Schneider and Georgakis, 2013).

3.2 Optimal control problem for the regulator

The NMPC uses a regulator that is based on certainty equivalence and a weighted least-squares objective with regularization on the inputs and the input rate-of-movement. This regulator can be expressed as the optimal control problem

$$\min_{x,u} \ \phi_k = \phi_{z,k} + \phi_{u,k} + \phi_{\Delta u,k}, \tag{33a}$$

$$s.t. \quad x(t_k) = \hat{x}_{k|k}, \tag{33b}$$

$$\dot{x}(t) = f(x(t), u(t), p), \quad t_k \le t \le t_k + T_p, \tag{33c}$$

$$z(t) = h(x(t), p), \quad t_k \le t \le t_k + T_p, \tag{33d}$$

$$u(t) = u_{k+j|k}, \quad j \in \mathcal{N}, \quad t_{k+j} \le t < t_{k+1+j}, \tag{33e}$$

$$u_l \le u_{k+j|k} \le u_u, \quad j \in \mathcal{N}, \tag{33f}$$

$$\Delta u_l \le \Delta u_{k+j|k} \le \Delta u_u, \quad j \in \mathcal{N}, \tag{33g}$$

with the objective function terms

$$\phi_{z,k} = \frac{1}{2}\int_{t_k}^{t_k+T_p} \|z(t) - \bar{z}(t)\|_{Q_z}^2 \,\mathrm{d}t, \tag{34a}$$

$$\phi_{u,k} = \frac{1}{2}\int_{t_k}^{t_k+T_p} \|u(t) - \bar{u}(t)\|_{Q_u}^2 \,\mathrm{d}t, \tag{34b}$$

$$\phi_{\Delta u,k} = \frac{1}{2}\sum_{j=0}^{N-1} \|\Delta u_{k+j}\|_{\bar{Q}_{\Delta u}}^2. \tag{34c}$$

We use a prediction and control horizon, T_p, that is defined by $T_p = NT_s$, where T_s is the sampling time and N is the discrete prediction and control horizon. We also use $\mathcal{N} = \{0, 1, \ldots, N-1\}$, $t_{k+j} = t_k + jT_s$ for $j \in \mathcal{N}$, and $t_{k+j+1} = t_{k+j} + T_s$. To have a consistent tuning in the limit $T_s \to 0$, we compute the rate-of-movement penalty as $\bar{Q}_{\Delta u} = Q_{\Delta u}/T_s$. We use $Q_z = 1$, $Q_u = 0$, $\bar{Q}_{\Delta u} = 10^6$, $T_s = 1$ s, $N = 10$, $u_l = 0$, $u_u = 1000$ mL/min, $\Delta u_l = -1000$ mL/min, and $\Delta u_u = 1000$ mL/min.

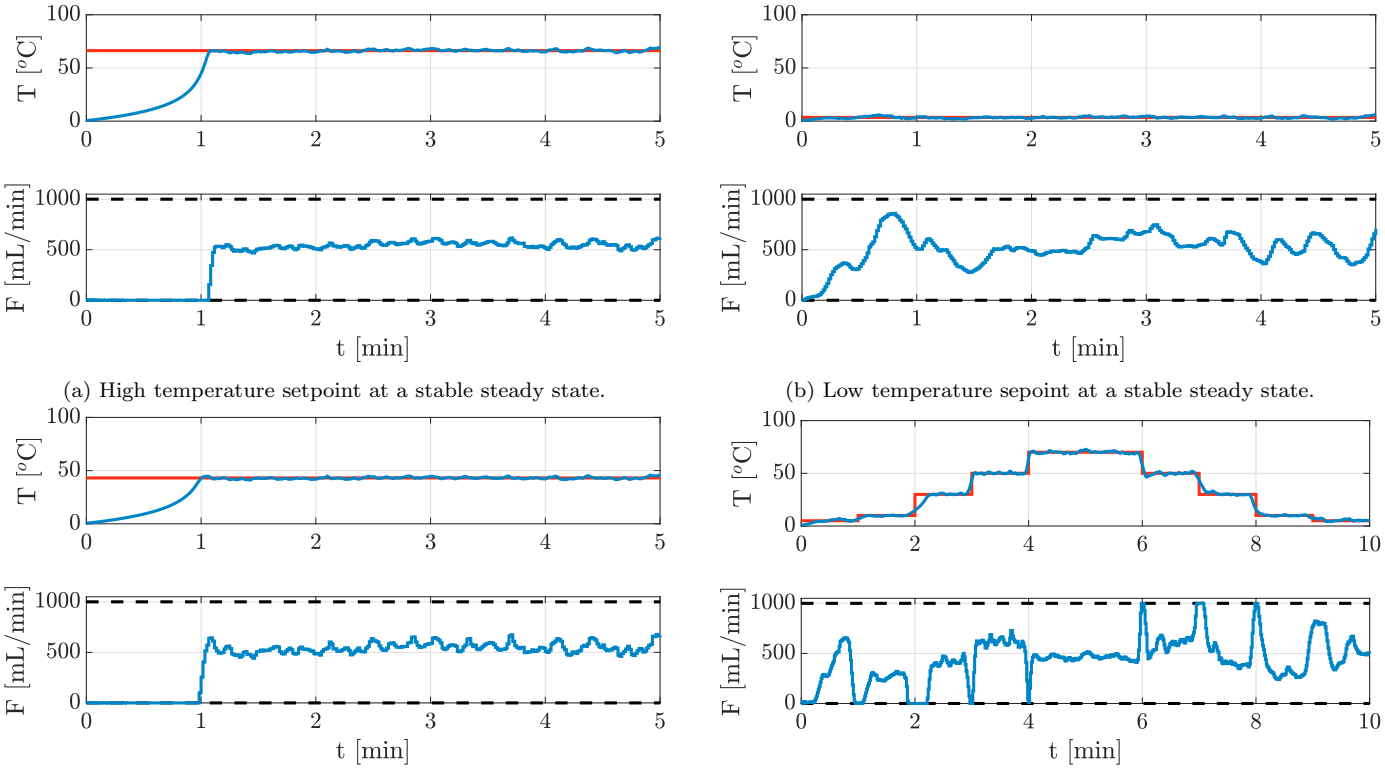

(a) High temperature setpoint at a stable steady state.

(b) Low temperature sepoint at a stable steady state.

(c) Medium temperature setpoint at an unstable steady state.

(d) Temperature setpoints at stable and unstable steady states.

Fig. 6. Closed-loop simulations with the NMPC for the adiabatic CSTR at different temperature setpoint trajectories. The NMPC is able to track any temperature setpoint in the entire temperature operation window of the adiabatic CSTR. It is able to track temperature setpoints at stable as well as unstable steady states.

The result of the optimal control problem is the parameters, $\{\hat{u}_{k+j|k}\}_{j=0}^{N-1}$, that defines the optimal trajectory for the manipuated variables, $u(t)$, the corresponding states, $x(t)$, and the outputs, $z(t)$, for $t_k \leq t \leq t_k + T_p$. Only the input corresponding to the first control interval is implemented, i.e.

$$u(t) = u_k = \hat{u}_{k|k}, \qquad t_k \leq t < t_{k+1} = t_k + T_s. \tag{35}$$

3.3 Closed-loop simulation

Fig. 6 shows closed-loop simulations for different temperature set point trajectories. The NMPC is able to stabilize any temperature setpoint.

4. CONCLUSION

The paper presents an NMPC algorithm based on a continuous-discrete stochastic reduced order model, and demonstrates that this control algorithm is able to track any temperature setpoint of a simulated exothermic reaction in an adiabatic CSTR. The system is simulated by a full order SDE model that is also developed and analyzed.

REFERENCES

Bindlish, R. (2015). Nonlinear model predictive control of an industrial polymerization process. *Computers and Chemical Engineering*, 73, 43–38.

Boiroux, D. and Jørgensen, J.B. (2018). Nonlinear model predictive control and artificial pancreas technologies. In *2018 IEEE Conference on Decision and Control (CDC)*, 284–290.

Brok, N.L., Madsen, H., and Jørgensen, J.B. (2018). Nonlinear model predictive control for stochastic differential equation systems. *IFAC-PapersOnLine*, 51(20), 430–435.

Forbes, M.G., Patwardhan, R.S., Hamadah, H., and Gopaluni, R.B. (2015). Model predictive control in industry: Challenges and opportunities. *IFAC-PapersOnLine*, 48(8), 531–538.

Honc, D., K., R.S., Abraham, A., Dusek, F., and Pappa, N. (2016). Teaching and practicing model predictive control. *IFAC-PapersOnLine*, 49(6), 034–039.

Qin, S.J. and Badgwell, T.A. (2003). A survey of industrial model predictive control technology. *Control Engineering Practice*, 11, 733–764.

Ritschel, T.K.S. and Jørgensen, J.B. (2019). Nonlinear model predictive control for disturbance rejection in isoenergetic-isochoric flash processes. *IFAC-PapersOnLine*, 52(1), 796–801.

Schneider, R. and Georgakis, C. (2013). How to NOT make the extended Kalman filter fail. *Ind. Eng. Chem. Res.*, 52, 3354–3362.

Schroll-Fleischer, E., Wu, H., Huusom, J.K., and Jørgensen, J.B. (2017). Adiabatic continuous stirred tank reactor. Technical report, Technical University of Denmark.

Vejtasa, S.A. and Schmitz, R.A. (1970). An Experimental Study of Steady State Multiplicity and Stability in an Adiabatic Stirred Reactor. *AIChE Journal*, 16(3), 410–419.